Noninvasive imaging of protein–protein interactions in living animals

Gary D. Luker*†, Vijay Sharma*†, Christina M. Pica*†, Julie L. Dahlheimer*†, Wei Li*†, Joseph Ochesky*†, Christine E. Ryan‡§, Helen Piwnica-Worms‡§¶, and David Piwnica-Worms*†‖

*Molecular Imaging Center, Mallinckrodt Institute of Radiology and Departments of †Molecular Biology and Pharmacology, ‡Cell Biology and Physiology, and ¶Internal Medicine, and §Howard Hughes Medical Institute, Washington University School of Medicine, St. Louis, MO 63110

Edited by Marcus E. Raichle, Washington University School of Medicine, St. Louis, MO, and approved March 19, 2002 (received for review January 14, 2002)

Protein–protein interactions control transcription, cell division, and cell proliferation as well as mediate signal transduction, oncogenic transformation, and regulation of cell death. Although a variety of methods have been used to investigate protein interactions *in vitro* and in cultured cells, none can analyze these interactions in intact, living animals. To enable noninvasive molecular imaging of protein–protein interactions *in vivo* by positron-emission tomography and fluorescence imaging, we engineered a fusion reporter gene comprising a mutant herpes simplex virus 1 thymidine kinase and green fluorescent protein for readout of a tetracycline-inducible, two-hybrid system *in vivo*. By using micro-positron-emission tomography, interactions between p53 tumor suppressor and the large T antigen of simian virus 40 were visualized in tumor xenografts of HeLa cells stably transfected with the imaging constructs. Imaging protein-binding partners *in vivo* will enable functional proteomics in whole animals and provide a tool for screening compounds targeted to specific protein–protein interactions in living animals.

Noncovalent associations between proteins regulate many essential biological processes, including transcription, translation, and metabolic or signal transduction pathways. The ability to investigate protein interactions has been revolutionized by development and application of techniques such as the yeast two-hybrid system (1), split ubiquitin (2), and protein fragment complementation (3, 4). Although existing technologies have provided important insights about composition and regulation of protein complexes, studies of protein interactions have been limited to assays *in vitro* and in cultured cells. Thus, development and application of methods to noninvasively image protein interactions *in vivo* would aid determinations of how the intricate regulatory pathways that exist in an intact animal modify binding specificities of proteins.

Recent studies have shown that positron-emission tomography (PET) imaging can be used to detect reporter proteins such as herpes simplex virus 1 thymidine kinase (HSV-1-TK) *in vivo* (5, 6). Nucleoside analogs, including 8-fluoroganciclovir (FGCV) (5), 5-iodo-2′-fluoro-1-β-D-arabinofuranosyluracil (FIAU) (7), and 9-(4-fluoro-3-hydroxymethylbutyl)guanine (FHBG) (8), are actively transported into cells and preferentially phosphorylated by the viral rather than mammalian thymidine kinase. Retention of phosphorylated nucleoside analogs correlates directly with expression of HSV-1-TK, and the nucleoside, when radiolabeled with a positron-emitting isotope, enables detection and quantification of the reporter protein by PET imaging (9, 10).

To develop a method for detecting protein–protein interactions in living mice, we combined the two-hybrid system with reporter proteins suitable for imaging (11, 12) (Fig. 1). A novel mutant HSV-1-TK fused to green fluorescent protein (GFP) was used as a reporter for imaging with both PET and optical techniques, whereas a tetracycline-inducible bidirectional promoter was used to regulate expression of the p53 tumor suppressor protein and TAg from simian virus 40 (SV40; ref. 13). By using micro-PET (14), we show that specific binding of p53 and TAg can be detected and quantified in living mice.

Materials and Methods

Construction of Plasmids. The N terminus nuclear localization sequence (NLS) of HSV-1-sr39TK (gift of H. Herschman, Univ. of California, Los Angeles, School of Medicine) was mutated to R25G–R26S by using 5′-GGGCGCAACGCCGTACTTCCGTTGCTATGGCCGCG-3′ and 5′-CGCGGCCATAGCAACGGAAGTACGGCGTTGCGCCC-3′ with the Quik-Change site-directed mutagenesis kit (Stratagene), creating mNLS-sr39TK. HSV-1-sr39TK and mNLS-sr39TK were digested with *Bam*HI and *Not*I and ligated to corresponding sites in pEGFP-N1 (CLONTECH) that previously were digested to remove EGFP. To create fusions with the N terminus of EGFP, flanking *Eco*RI and *Bam*HI restriction sites were added to HSV-1-sr39TK and mNLS-sr39TK by PCR by using the primers 5′-TCGCCCTTAGAATTCGCCACCATGG-3′ and 5′-TCACCGGATCCCAGTTAGCCTCCCCCATCTCCCGG-3′, and the resulting cDNAs were ligated to corresponding sites in native pEGFP-N1. PCR products were verified by sequencing. The cytomegalovirus promoter from pcDNA6/V5-HisA (Invitrogen) was replaced with the Gal4 promoter from pG5CAT (CLONTECH), and mNLS-sr39TK-EGFP was inserted into the resultant plasmid to produce the Gal4-mNLS-sr39TK-EGFP reporter gene. The reverse tetracycline-controlled transactivator rtTA2^S-M2 (gift of W. Hillen, Universität Erlangen, Germany) was inserted into the *Eco*RI and *Not*I sites of pIRESneo (CLONTECH), producing pIRES-rtTA2^S-M2. Plasmids pBI/Gal4-BD-p53/VP16-TAg and pBI/Gal4-BD-p53/VP16-CP were constructed by inserting fusions of Gal4 DNA-binding domain with p53 and VP16 activation domain with SV40 TAg or polyoma virus coat protein (CP) (Mammalian Matchmaker Two-Hybrid Assay kit; CLONTECH) into the *Not*I (blunted) and *Sal*I sites (Gal4-BD-p53) and *Sac*II site (blunted) (VP16 fusions) of pBI, respectively (CLONTECH). pBI contains a tetracycline-responsive element that enables bidirectional, tetracycline-inducible expression of pairs of hybrid proteins.

Generation of Recombinant Adenoviruses. Gal4-BD-p53, VP16-TAg, and VP16-CP were inserted into the *Bgl*II and *Xba*I sites of pShuttle cytomegalovirus (gift of B. Vogelstein, Johns Hopkins Univ., Baltimore) and coelectroporated with pAdEasy-1

This paper was submitted directly (Track II) to the PNAS office.

Abbreviations: PET, positron-emission tomography; HSV-1-TK, herpes simplex virus 1 thymidine kinase; SV40, simian virus 40; GFP, green fluorescent protein; CP, coat protein; 8-^{3}H-PCV, 8-^{3}H-penciclovir; ^{18}F-FHBG, 9-(4-[^{18}F]-fluoro-3-hydroxymethylbutyl)guanine; NLS, nuclear localization sequence(s).

‖To whom reprint requests should be addressed at: Molecular Imaging Center, Mallinckrodt Institute of Radiology, Washington University School of Medicine, Box 8225, 510 South Kingshighway Boulevard, St. Louis, MO 63110. E-mail: piwnica-wormsd@mir.wustl.edu.

The publication costs of this article were defrayed in part by page charge payment. This article must therefore be hereby marked "*advertisement*" in accordance with 18 U.S.C. §1734 solely to indicate this fact.

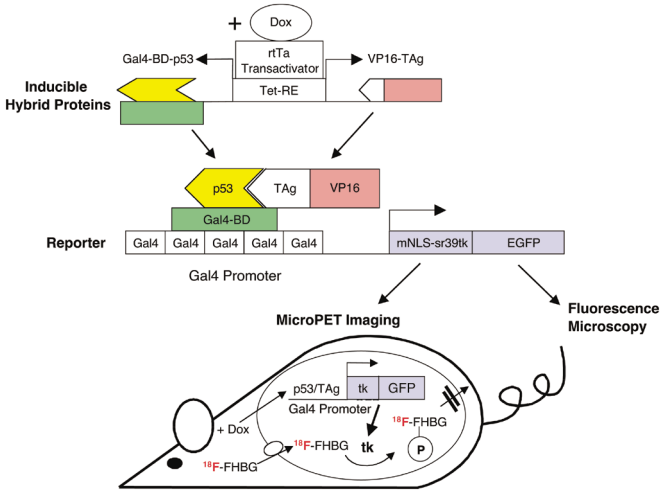

Fig. 1. Strategy for imaging protein–protein interactions *in vivo*. Treatment with doxycycline activates a constitutively expressed reverse tetracycline-responsive transactivator to induce bidirectional transcription of Gal4-BD-p53 and VP16-TAg, hybrid proteins containing the target proteins p53 and TAg fused to the yeast Gal4 DNA-binding domain and the HSV-1 VP16 activation domain, respectively. Interaction of p53 and TAg assembles the hybrid transcriptional activator on the Gal4 promoter, inducing transcription of the mNLS-sr39TK-EGFP reporter. The fusion reporter protein can be detected by micro-PET imaging of living mice by using TK-mediated phosphorylation (P) and intracellular trapping of the positron-emitting radiopharmaceutical ^{18}F-FHBG or by fluorescence imaging of GFP.

into *Escherichia coli* BJ5183 to achieve homologous recombination. Recombinant adenoviruses were generated and propagated with the AdEasy system (15).

Cell Culture and Transfection. HeLa cells were grown in DMEM with 10% (vol/vol) heat-inactivated FBS, 1% (vol/vol) glutamine, and 0.1% penicillin-streptomycin. Transfections were performed with Fugene 6 (Roche, Gipf-Oberfrick, Switzerland). The reporter cell line (HeLa-Gal4-mNLS-sr39TK-EGFP) was produced by sequential transfection of Gal4-mNLS-sr39TK-EGFP and pIRES-rtTA2^S-M2, using 2.5 μg/ml blasticidin and 500 μg/ml G418, respectively, to select clonal cell lines. A single clone containing both plasmids then was cotransfected with either pBI/Gal4-BD-p53/VP16-TAg or pBI/Gal4-BD-p53/VP16-CP and a hygromycin resistance plasmid (pTK-Hyg, CLONTECH) at a molar ratio of 20:1. Clonal cell lines with Gal4-mNLS-sr39TK-EGFP, pIRES-rtTA2^S-M2, and either pBI/Gal4-BD-p53/VP16-TAg or pBI/Gal4-p53/VP16-CP were selected with 50 μg/ml hygromycin in medium containing Tet-system approved FBS (CLONTECH). Resultant cell lines with Gal4-BD-p53/VP16-TAg or Gal4-BD-p53/VP16-CP were designated as TAg or CP cells, respectively.

Radiochemicals. 8-^{3}H-penciclovir (8-^{3}H-PCV; 14.9 Ci/mmol) was obtained from Moravek Biochemicals (Brea, CA). 9-(4-[^{18}F]-Fluoro-3-hydroxymethylbutyl)guanine (^{18}F-FHBG; ≈300 Ci/mmol) was synthesized in the Washington University Molecular Imaging Center Chemistry Core, as described (16), by using a modified procedure of the synthesis reported by Alauddin and Conti (8).

***In Vitro* Radiotracer Assays.** Cell uptake of 8-^{3}H-PCV (0.2 μCi/ml) or ^{18}F-FHBG (5–10 μCi/ml) was performed 48 h after transient transfection of cells, 24 h after adenoviral infection at a multiplicity of infection of 10, or at various time periods after incubation with doxycycline (1 μg/ml) as described in the figure legends (16). Data were expressed as moles of nucleoside analog/mg P per nM$_o$, where mg P refers to mg of cell protein and nM$_o$ is the concentration of nucleoside analog in the extracellular space (17); data from transient transfections were normalized to cotransfected β-galactosidase instead of mg P. Data were reported as means ± SE. Pairs were compared by Student's t test. Values of $P \leq 0.05$ were considered significant (18).

Western Blotting. Western blotting was performed to determine expression of Gal4-BD-p53, VP16-TAg, and VP16-CP in cells and tumors (19) by using primary antibodies to the Gal4-binding domain and VP16 activation domain (CLONTECH). Immune complexes were detected with goat anti-mouse and anti-rabbit secondary antibodies, respectively, coupled to alkaline phosphatase (Santa Cruz Biotechnology).

Fluorescence Microscopy. Tumor specimens were snap-frozen in Tissue-Tek OCT compound (Sakura, Torrance, CA) and cryosectioned. Tumors and cultured cells were processed for fluorescence microscopy as described (20).

Animal Studies. Animal care and euthanasia were approved by the Washington University Medical School Animal Research Committee. Gal4-BD-p53/VP16-TAg cells (1.5×10^7) or Gal4-BD-p53/VP16-CP cells (1×10^7) were injected s.c. into each axilla of adult NCr *nu/nu* mice (Taconic Farms). After ≈5-mm tumors developed, mice were treated with i.p. injections of doxycycline (60 μg/g body weight) in PBS or PBS alone. Doses were administered at 6- to 8-h intervals for various times, with the total number of doses and time before imaging indicated in the figure legends. For micro-PET imaging (Concorde MicroSystems, Knoxville, TN), mice were anesthetized lightly with isofluorane before tail vein injection of ^{18}F-FHBG (≈95 μCi; 1 Ci = 37 GBq) and allowed to recover. Mice again were anesthetized with isofluorane 1 h later, placed supine within the micro-PET scanner, and imaged (10–20 min of acquisition time; one bed position; filtered-back projection reconstruction; isotropic image resolution of 1.8 mm). Micro-PET images were corrected for decay but not attenuation, and regions of interest (ROI) were analyzed with ANALYZEPC 3.0 software. ROI counts were converted to counts per gram of tissue (nCi/g), assuming a tissue density of 1 g/ml, and standard uptake values for each tumor were calculated from the imaging data by dividing the counts per gram of tissue by injected dose of radioactivity per gram of animal weight. Because CP tumors could not be identified by imaging with ^{18}F-FHBG, ROI counts obtained from tissues near the expected position of the CP tumor were used for negative control values. Similarly, animals were anesthetized with metofane and biodistribution studies were performed 1 h after tail vein injection of ^{18}F-FHBG (≈15 μCi). Immediately after removal of tumors and selected organs, tissues were assayed for radioactivity (Cobra II; Beckman Coulter) and weighed. Radiotracer content was expressed as percent injected dose per gram of tissue (% ID/g) (21). Tumor content of ^{18}F-FHBG was normalized to accumulation of radiotracer in heart, a representative background organ that does not significantly accumulate ^{18}F-FHBG (22).

Results

Enhanced HSV-1-TK Reporter Protein. As a first step toward imaging protein–protein interactions *in vivo*, we engineered HSV-1-TK to improve its sensitivity as a reporter gene for imaging. Previous mutagenesis of wild-type HSV-1-TK led to isolation of HSV-1-sr39TK (23), a mutant with improved sensitivity for imaging with 8-^{18}F-fluoropenciclovir (9), whereas other investigators demonstrated that mutations in one of three putative NLS of HSV-1-TK (24) conferred greater uptake of ^{124}I-FIAU

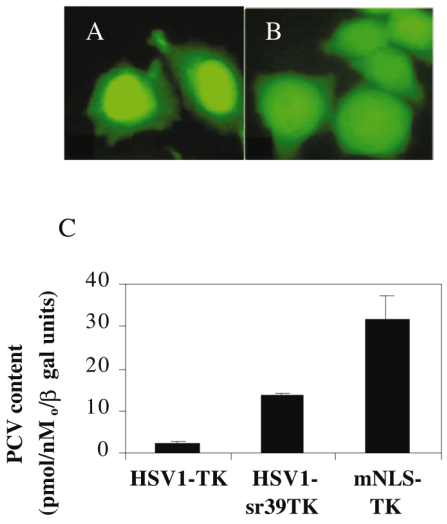

Fig. 2. Expression of various HSV-1-TK reporter proteins in transiently transfected HeLa cells. (*A* and *B*) Fluorescence micrographs (×400) show predominantly nuclear localization of HSV-1-sr39TK-EGFP (*A*), whereas mNLS-sr39TK-EGFP is distributed more uniformly throughout the nucleus and cytosol (*B*). (*C*) Cell accumulation of 8-^{3}H-PCV is greatest in cells transfected with mNLS-sr39TK ($P < 0.05$; $n = 3$ each, representative of three independent experiments).

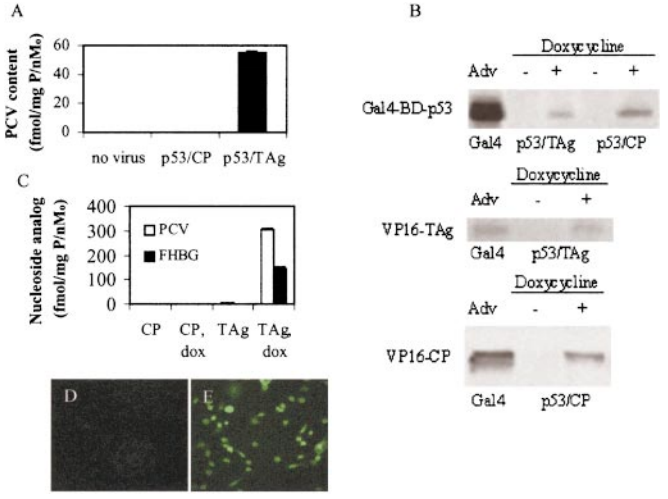

Fig. 3. Characterization of the imaging two-hybrid system *in vitro*. (*A*) HeLa-Gal4 reporter cells were mock-infected or infected with adenoviruses expressing Gal4-BD-p53 and VP16-TAg or VP16-CP. Cells infected with the interacting pair of proteins had significantly increased accumulation of 8-^{3}H-PCV ($P < 0.0001$; $n = 4$ each, representative of three independent experiments). (*B*) Western blotting of hybrid proteins in HeLa-Gal4 reporter cells after adenoviral infection or in TAg cells (with Gal4-BD-p53 and VP16-TAg) and CP cells (with Gal4-BD-p53 and VP16-CP) 48 h after treatment with doxycycline (1 μg/ml) (+) or vehicle alone (−). (*C*) Cell content of 8-^{3}H-PCV and ^{18}F-FHBG is significantly greater in TAg cells after induction of interacting proteins with doxycycline (dox) for 48 h ($P < 0.0001$; $n = 4$ each, representative of four experiments for 8-^{3}H-PCV and one experiment for ^{18}F-FHBG). (*D* and *E*) Fluorescence micrographs (×100) of TAg cells without (*D*) or with (*E*) doxycycline-mediated induction of interacting hybrid proteins. Expression of mNLS-sr39TK-EGFP is seen only in cells treated with doxycycline.

(25). Therefore, we disrupted the N terminus NLS of HSV-1-sr39TK by changing arginines (R) 25 and 26 to glycine (G) and serine (S) (24), respectively, to create mNLS-sr39TK. To enable subcellular localization of each reporter gene, we fused EGFP to HSV-1-sr39TK or mNLS-sr39TK. By fluorescence microscopy, HSV-1-sr39TK-EGFP was observed predominantly in the nucleus of transiently transfected HeLa cells (Fig. 2*A*). Conversely, mNLS-sr39TK-EGFP was distributed more uniformly in both nucleus and cytosol (Fig. 2*B*), consistent with disruption of one NLS. Next, we determined whether disrupting the N terminus NLS of HSV-1-sr39TK enhanced accumulation of the radiolabeled nucleoside analog 8-^{3}H-PCV. HeLa cells were transfected transiently with each reporter construct for 48 h and then incubated with 8-^{3}H-PCV (0.2 μCi/ml) for 1 h, followed by a 1-h chase in radiotracer-free medium to quantify retained phosphorylated nucleoside (16). Content of radiotracer in cells expressing mNLS-sr39TK was more than 2-fold greater than HSV-1-sr39TK and 12-fold greater than wild-type HSV-1-TK (Fig. 2*C*). These data indicated that mutating the NLS of HSV-1-sr39TK enhanced nucleoside trapping by the reporter protein, thus conferring greater sensitivity for imaging protein interactions *in vivo*.

Characterization of the Two-Hybrid System *in Vitro*. We selected the well characterized interaction between p53 tumor suppressor protein and TAg of SV40 as the model to validate our imaging system (Fig. 1). p53 protein is nonfunctional in greater than 50% of human cancers (26), and TAg is the transforming protein of SV40 virus (27). TAg binds constitutively to p53 and blocks transactivation of target genes by p53, leading to transformation of mammalian cells (13). p53 and TAg were fused to the Gal4 DNA-binding domain from *Saccharomyces cerevisiae* (Gal4-BD-p53) and the VP16 activation domain from HSV-1 (VP16-TAg), respectively (Fig. 1). A hybrid protein of VP16 and polyoma virus coat protein (VP16-CP), which does not bind to p53, was used as a negative control. To enable detection of protein interactions by radiotracer and optical techniques, we used mNLS-sr39TK-EGFP as the reporter, placed downstream of a promoter composed of five copies of Gal4 DNA-binding sites and a minimal TATA box promoter (Gal4-mNLS-sr39TK-EGFP) (28).

To develop a reporter cell line for *in vivo* imaging, we stably transfected HeLa cells with Gal4-mNLS-sr39TK-EGFP. By using adenoviruses to express pairs of positive (Gal4-BD-p53, VP16-TAg) and negative (Gal4-BD-p53, VP16-CP) interacting proteins, we quantified cellular accumulation of 8-^{3}H-PCV to identify a cell line (HeLa-Gal4) with low background expression and high induction of the reporter protein (Fig. 3*A*). Mock infected (no virus) HeLa-Gal4 cells and HeLa-Gal4 cells expressing Gal4-BD-p53 and VP16-CP did not accumulate nucleoside analog above background levels (threshold of detection, ≈0.2 fmol PCV/mg P per nM_o). In contrast, cells expressing Gal4-BD-p53 and VP16-TAg accumulated nucleoside analog to 55.2 ± 0.6 fmol PCV/mg P per nM_o ($P < 0.0001$). These data show that the HeLa-Gal4 reporter cells could be used to detect interactions between p53 and SV40 TAg in cultured cells.

To enable inducible expression of hybrid proteins *in vitro* and *in vivo*, we stably transfected HeLa-Gal4 reporter cells with a reverse tetracycline-responsive transactivator expressed from a cytomegalovirus promoter and a plasmid expressing either Gal4-BD-p53 and VP16-TAg or Gal4-BD-p53 and VP16-CP from a bidirectional, tetracycline-regulated promoter. Clonal cell lines with either the positive (Gal4-BD-p53/VP16-TAg) or negative (Gal4-BD-p53/VP16-CP) interacting proteins (TAg cells and CP cells, respectively) were treated with doxycycline (1 μg/ml) for 48 h before analyzing protein expression by Western blotting (Fig. 3*B*). We detected hybrid proteins only after incubation with doxycycline, demonstrating tightly regulated expression of the target genes. To quantify activity of the reporter, we measured cell content of 8-^{3}H-PCV or ^{18}F-FHBG after incubating cells with doxycycline for 48 h to induce the negative and positive

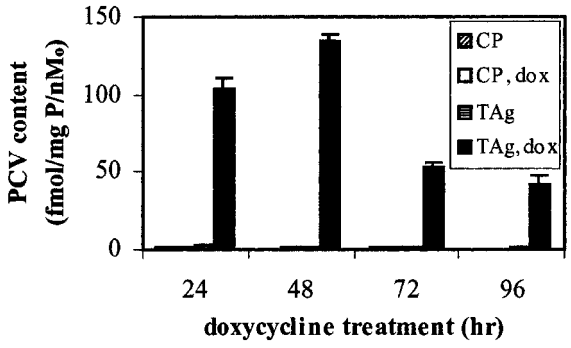

Fig. 4. Time course of reporter protein induction in cultured cells. Net content of 8-^{3}H-PCV in CP and TAg cells without or with doxycycline (dox) induction for 24–96 h. Accumulation of PCV is absent in CP cells and greatest in TAg cells after inducing interacting proteins for 48 h with doxycycline ($P < 0.02$; $n = 4$ each).

interacting proteins (Fig. 3*C*). In CP cells, content of each nucleoside analog remained at background levels both in the absence and presence of doxycycline. In contrast, function of the reporter increased by approximately 76- and 190-fold as measured with 8-^{3}H-PCV and ^{18}F-FHBG, respectively, after inducing expression of hybrid proteins in TAg cells ($P < 0.0001$). Absolute retention of ^{18}F-FHBG was approximately 50% less than 8-^{3}H-PCV, possibly because of replacement of one pendant hydroxyl group in PCV with ^{18}F in ^{18}F-FHBG, thus eliminating one potential phosphorylation site for the mNLS-sr39TK enzyme.

We also examined expression of the GFP component of the reporter by fluorescence microscopy. Consistent with data from radiotracer assays, no GFP fluorescence was observed in CP cells with or without doxycycline (data not shown) and in TAg cells without doxycycline (Fig. 3*D*). However, we readily detected GFP in all TAg cells after doxycycline induction (Fig. 3*E*), showing that positive protein–protein interactions also could be detected *in vitro* by fluorescence imaging.

To determine the time course of reporter gene induction, we incubated cells with doxycycline (1 μg/ml) for 24–96 h before measuring accumulation of 8-^{3}H-PCV (Fig. 4). Compared with untreated or treated CP cells or untreated TAg cells, content of 8-^{3}H-PCV increased by 37- and 149-fold in TAg cells treated with doxycycline for 24 and 48 h, respectively. After peaking at 48 h, reporter activity decreased at 72 and 96 h. Overall, these data demonstrated that specific interactions between two proteins could be detected and quantified with the inducible two-hybrid system *in vitro*, by using a reporter gene and a radiolabeled nucleoside analog that would enable micro-PET imaging.

Imaging Protein Interactions *in Vivo*. To determine the feasibility of imaging two-protein interactions in living animals, we produced xenograft tumors of TAg and CP cells in the axillae of *nu/nu* mice. After tumors grew to a diameter of ≈5 mm, we treated mice with doxycycline for 48 h to induce expression of hybrid proteins and then imaged mice 1 h after tail vein injection of ^{18}F-FHBG to detect the Gal4-mNLS-sr39TK-EGFP reporter (Fig. 5 *A* and *B*). Accumulation of radiotracer was evident in the TAg tumor, but not in the CP tumor, showing that specific interaction of p53 and TAg could be detected by micro-PET imaging. Based on region-of-interest values from the micro-PET images, which have been proven to reflect accurately tissue content of radiotracer (14), uptake of ^{18}F-FHBG was 5.5-fold greater in TAg tumors relative to CP tumors (Fig. 5*C Inset*; $P < 0.01$).

To directly correlate data obtained *in vitro* and *in vivo*, we performed biodistribution studies in *nu/nu* mice with xenograft tumors of TAg and CP cells. Without doxycycline, accumulation of ^{18}F-FHBG did not differ between TAg and CP tumors (Fig. 5*C*). However, treatment with doxycycline for 48 h increased uptake of ^{18}F-FHBG in TAg tumors by 5.8-fold over CP tumors ($P < 0.001$), comparable to micro-PET imaging. ^{18}F-FHBG content did not change significantly in control CP tumors. Fluorescence microscopy of the excised tumors revealed expression of GFP in doxycycline-treated TAg tumors *in vivo* (Fig. 5*D*) but not in untreated or control tumors. Fluorescence images were consistent with both micro-PET and biodistribution data while also showing heterogeneous expression of the reporter within tumor specimens *in vivo*. Western blotting confirmed that hybrid proteins were induced *in vivo* in both tumor xenografts (data not shown).

To determine whether micro-PET imaging can quantify relative differences in amounts of interacting proteins, we treated mice bearing TAg and CP tumor xenografts with doxycycline for 12, 24, and 48 h before micro-PET imaging (Fig. 5 *E–G*) or biodistribution studies (Fig. 5*H*) with ^{18}F-FHBG. In response to doxycycline, Western blotting of excised tumor samples confirmed time-dependent increases in expression of all hybrid proteins (Gal4-BD-p53, VP16-TAg, and VP16-CP) (data not shown). Both imaging and biodistribution studies showed proportional increases in accumulation of radiotracer over time only in TAg tumors, whereas content of nucleoside analog did not change in CP tumors (Fig. 5*H*). In the absence of doxycycline, no accumulation of radiotracer above background levels could be detected in either tumor by micro-PET imaging. These data directly demonstrated that the imaging two-hybrid system responded in a proportional fashion to increasing amounts of interacting proteins *in vivo*.

Discussion

We developed a technique for noninvasive imaging of protein–protein interactions *in vivo* by combining the two-hybrid system with recently developed technologies for monitoring reporter probes in living animals. Specific binding of p53 to SV40 TAg induced expression of a reporter gene composed of a novel mutant HSV-1-TK fused to GFP. In the absence of interacting proteins, or in the presence of proteins that did not bind, function of the reporter essentially was at background levels both in cultured cells and in tumors *in vivo*. By using micro-PET imaging with ^{18}F-FHBG, we detected binding of p53 and TAg in living mice and quantified an ≈6-fold enhancement of mNLS-sr39TK activity in response to interactions of these two proteins *in vivo*. These imaging data were confirmed with direct measurements of radiotracer content in tumors, demonstrating that micro-PET accurately represents differences in function of the mNLS-sr39TK-EGFP reporter for the imaging two-hybrid system. Significantly, function of the reporter protein, as measured by accumulation of nucleoside analog, was enhanced with increasing amounts of interacting proteins (Fig. 5 *E–H*). Potentially, relative differences in affinity between proteins, which can be determined with two-hybrid systems *in vitro* from levels of reporter protein activity (29), could be measured in living animals by using micro-PET imaging. Further studies will be needed to determine the limitations of the system for imaging "weak" protein interactions and to define the kinetics of the system for detecting temporal changes in protein–protein binding.

The GFP component of the fusion reporter gene also could be detected upon binding of p53 and SV40 TAg *in vitro* and *in vivo*. Although we monitored expression of GFP both in cells and excised tumors by fluorescence microscopy, recent studies have shown the feasibility of noninvasively imaging GFP in living mice (30). External detection of GFP is limited currently to two-dimensional imaging and qualitative assessment of

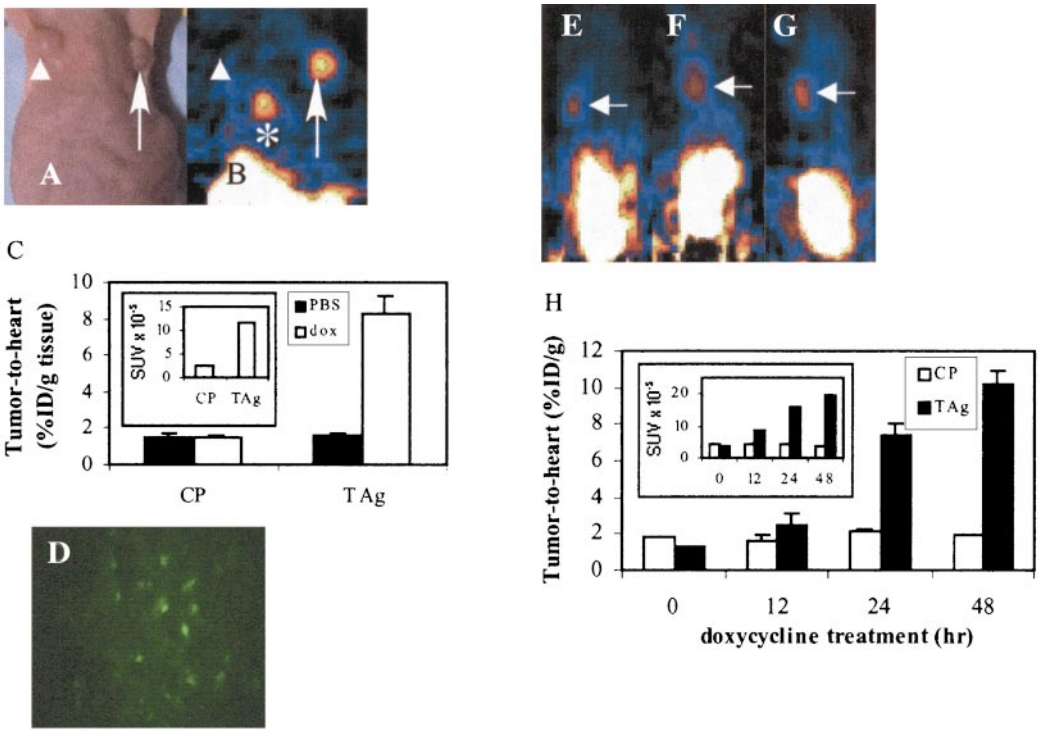

Fig. 5. Imaging protein interactions *in vivo*. (*A*) Photograph of the anterior thorax of a *nu/nu* mouse with axillary xenograft tumors of CP cells (arrowhead) and TAg cells (arrow). (*B*) Coronal micro-PET image of the same mouse 48 h after starting treatment with i.p. injections of doxycycline (dox; 60 μg/g body weight $\times$ six doses) showing accumulation of ^{18}F-FHBG only in the TAg tumor (arrow) expressing the interacting proteins Gal4-BD-p53 and VP16-TAg (representative image of three animals). Asterisk denotes radiotracer in the gallbladder. Intestinal activity from normal hepatobiliary clearance of the radiotracer is observed in the lower portion of the image. (*C*) Quantitative biodistribution of ^{18}F-FHBG in mice bearing TAg and CP tumors, using the protocol described in *B* for i.p. administration of doxycycline or PBS alone over 48 h ($n = 3$–4 each). Accumulation of ^{18}F-FHBG in doxycycline-treated TAg tumors was significantly greater than all other conditions ($P < 0.001$). *Inset* shows quantitation of radiotracer accumulation from micro-PET images, expressed as standard uptake values (SUV) $\times 10^{-5}$. (*D*) Fluorescence micrograph ($\times$100) of a TAg tumor specimen from a mouse treated with doxycycline. (*E*–*G*) Sagittal micro-PET images of TAg tumors (arrows) performed after i.p. administration of doxycycline (60 μg/g body weight) for 12 h [two doses of dox (*E*)], 24 h [three doses of dox (*F*)], or 48 h [six doses of dox (*G*)]. (*H*) Quantitative data for biodistribution of ^{18}F-FHBG in TAg and CP tumors in the absence of doxycycline or 12, 24, and 48 h after administration of drug, using the same dosing protocol as for *E*–*G*. *Inset* shows SUV data calculated from micro-PET images.

levels of reporter protein, unlike the three-dimensional, quantitative detection of reporter activity with PET. Nonetheless, imaging of GFP *in vivo* could provide a rapid screening assay for detecting the presence or absence of protein–protein interactions, thus increasing the throughput of the imaging two-hybrid system for monitoring responses to various experimental conditions.

We envision that imaging protein interactions *in vivo* will have broad applications in basic and translational research. Xenograft models may prove effective for initial characterization of drugs targeted to specific protein interactions because bioavailability, pharmacokinetics, and therapeutic validation of a compound can be screened simultaneously in a living animal. Development of transgenic mice with the reporter gene for the imaging two-hybrid system will allow protein interactions to be monitored in native organs and tissues, using viral or nonviral vectors to deliver and express proteins of interest. Molecular imaging of protein–protein interactions also will provide a broad-based platform for researchers to integrate existing knowledge of protein interactions within the complex physiological context of living animals. This has the potential to significantly advance our understanding of how protein interactions affect normal physiology, development, disease progression, and response to therapy *in vivo*.

We thank John Engelbach and Joon Young Kim for technical assistance and colleagues of the Washington University Research Resource for Isotope Research for production of ^{18}F. This work was supported by National Institutes of Health Grants P20 CA86251 and P50 CA94056 and Department of Energy Grant 94ER61885. H.P.W. is an Investigator of the Howard Hughes Medical Institute.

1. Fields, S. & Song, O. (1989) *Nature (London)* **340,** 245–246.
2. Johnsson, N. & Varshavsky, A. (1994) *Proc. Natl. Acad. Sci. USA* **91,** 10340–10344.
3. Rossi, F., Charlton, C. & Blau, H. (1997) *Proc. Natl. Acad. Sci. USA* **94,** 8405–8410.
4. Remy, I. & Michnick, S. (1999) *Proc. Natl. Acad. Sci. USA* **96,** 5394–5399.
5. Gambhir, S., Barrio, J., Herschman, H. & Phelps, M. (1999) *Nucl. Med. Biol.* **26,** 481–490.
6. Blasberg, R. & Tjuvajev, J. (1999) *Q. J. Nucl. Med.* **43,** 163–169.
7. Tjuvajev, J. G., Stockhammer, G., Desai, R., Uehara, H., Watanabe, K., Gansbacher, B. & Blasberg, R. G. (1995) *Cancer Res.* **55,** 6126–6132.
8. Alauddin, M. & Conti, P. (1998) *Nucl. Med. Biol.* **25,** 175–180.
9. Gambhir, S., Bauer, E., Black, M., Liang, Q., Kokoris, M., Barrio, J., Iyer, N., Namavari, M., Phelps, M. & Herschman, H. (2000) *Proc. Natl. Acad. Sci. USA* **97,** 2785–2790.
10. Bennett, J., Tjuvajev, J., Johnson, P., Doubrovin, M., Akhurst, T., Malholtra, S., Hackman, T., Balatoni, J., Finn, R., Larson, S., *et al.* (2001) *Nat. Med.* **7,** 859–863.
11. Tucker, C., Gera, J. & Uetz, P. (2001) *Trends Cell Biol.* **11,** 102–106.
12. Jacobs, A., Dubrovin, M., Hewett, J., Sena-Esteves, M., Tan, C., Slack, M., Sadelain, M., Breakefield, X. & Tjuvajev, J. (1999) *Neoplasia* **1,** 154–161.
13. Bargonetti, J., Reynisdottir, I., Friedman, P. & Prives, C. (1992) *Genes Dev.* **6,** 1886–1898.

14. Cherry, S., Shao, Y., Silverman, R., Meaders, K., Siegel, S., Chatzioannou, A., Young, J., Jones, W., Moyers, J., Newport, D., *et al.* (1997) *IEEE Trans. Nucl. Sci.* **44,** 1161–1166.
15. He, T., Zhou, S., da Costa, L., Yu, J., Kinzler, K. & Vogelstein, B. (1998) *Proc. Natl. Acad. Sci. USA* **95,** 2509–2514.
16. Luker, G., Luker, K., Sharma, V., Pica, C., Dahlheimer, J., Ocheskey, J., Fahrner, T., Milbrandt, J. & Piwnica-Worms, D. (2002) *Mol. Imaging* **1,** 65–73.
17. Piwnica-Worms, D., Rao, V., Kronauge, J. & Croop, J. (1995) *Biochemistry* **34,** 12210–12220.
18. Glantz, S. A. (1987) *Primer of Biostatistics* (McGraw—Hill, New York), 2nd Ed., p. 379.
19. Luker, K., Pica, C., Schreiber, R. & Piwnica-Worms, D. (2001) *Cancer Res.* **61,** 6540–6547.
20. Polyakov, V., Sharma, V., Dahlheimer, J., Pica, C., Luker, G. & Piwnica-Worms, D. (2000) *Bioconjugate Chem.* **11,** 762–771.
21. Sharma, V., Beatty, A., Wey, S.-P., Dahlheimer, J., Pica, C., Crankshaw, C., Bass, L., Green, M., Welch, M. & Piwnica-Worms, D. (2000) *Chem. Biol.* **7,** 335–343.
22. Alauddin, M., Shahinian, A., Gordon, E., Bading, J. & Conti, P. (2001) *J. Nucl. Med.* **42,** 1682–1690.
23. Black, M., Newcomb, T., Wilson, H. & Loeb, M. (1996) *Proc. Natl. Acad. Sci. USA* **93,** 3525–3529.
24. Degreve, B., Esnouf, R., De Clerq, E. & Balzarini, J. (1999) *Biochem. Biophys. Res. Commun.* **264,** 338–342.
25. Ponomarev, V., Dubrovin, M., Beresten, T., Balatoni, J., Blasberg, R. & Tjuvajev, J. (2000) *J. Nucl. Med.* **41,** 81P.
26. Hollstein, M., Sidransky, D., Vogelstein, B. & Harris, C. (1991) *Science* **253,** 49–53.
27. Schaffhausen, B. (1982) *CRC Crit. Rev. Biochem.* **13,** 215–286.
28. Carey, M., Leatherwood, J. & Ptashne, M. (1990) *Science* **247,** 710–712.
29. Albrecht, V., Ritz, O., Linder, S., Harter, K. & Kudla, J. (2001) *EMBO J.* **20,** 1051–1063.
30. Yang, M., Baranov, E., Jiang, P., Sun, F.-X., Li, X.-M., Li, L., Hasegawa, S., Bouvet, M., Al-Tuwaijri, M., Chishima, T., *et al.* (2000) *Proc. Natl. Acad. Sci. USA* **97,** 1206–1211.